Chapter 6

Photoluminescence Measurements of Quantum-Dot-Containing Microdisks Using Optical Fiber Tapers

The ability to efficiently couple light into and out of semiconductor microcavities is an important aspect of many microphotonic technologies [153], and plays a vital role in chip-based implementations of cavity quantum electrodynamics (cQED) for quantum networking and cryptography [60, 9, 154]. While some geometries, such as micropillar cavities, exhibit highly directional emission that can be effectively collected [16, 109], coupling to wavelength-scale semiconductor microcavities is in general non-trivial [120, 155, 156, 154], due to a number of factors. These include the size disparity between the modes of the microcavity and those of standard free-space and fiber optics, the refractive index difference between semiconductors and glass or air, and the potentially complicated cavity mode profiles sustained by these devices. In this thesis, we have presented evanescent coupling through optical fiber tapers as a way to couple efficiently to semiconductor microcavities. As we have already discussed, such fiber tapers have been used as near-ideal coupling channels for glass-to-glass coupling with silica-based microcavities such as microspheres [32, 157, 20, 55] and microtoroids [56]. In addition, as described in chapters 4 and 5, our recent experiments have indicated that they can also serve as efficient couplers to high-refractive index semiconductor-based devices, such as photonic crystal waveguides [39], photonic crystal cavities [52, 57] and microdisks [64, 69]. While the work described in the previous chapter primarily utilized fiber tapers for passive measurements such as the characterization of cavity quality factors, in this chapter, which is largely based on ref. [75], we focus on using the fiber taper as an efficient coupler for injecting pump light into and extracting the light emitted by semiconductor quantum dots into microdisk whispering gallery modes. The immediate device application that we study

here is room-temperature, fiber-coupled microdisk-quantum-dot lasers, but the results described are directly applicable to future studies of cavity QED phenomena in semiconductor-based systems.

In section 6.1, we qualitatively describe the issues addressed in this chapter, as well as the experimental setup we use. In section 6.2, we briefly review passive measurements in the 1200 nm wavelength band to determine the optical losses of the optical resonant cavities under study. In section 6.3, we present experimental results demonstrating the improvements that result when free-space collection is replaced by fiber-based collection in photoluminescence measurements, while in section 6.4, we present initial results on microdisk lasers that employ both fiber pumping and fiber collection. Finally, in section 6.5, we consider some of the applications of this work to future experiments.

6.1 Preliminary discussion and experimental methods

The free-space collection from a whispering gallery mode (WGM) of a microdisk is a function of a number of factors, including the position and numerical aperture (NA) of the collection lens, and the radiation pattern and quality factor (Q) of the resonant mode. Optical losses from the microdisk include not only the (ideal) radiation due to radial tunneling of light from the disk periphery, but also scattering losses due to surface roughness imperfections at the disk edge and material absorption. For high-refractive index ($n \sim 3.5$) III-V semiconductor microdisks, surface roughness scattering is typically the dominant form of radiation from the microcavity. The intrinsic radiation loss of semiconductor microdisks is almost negligible in all cases, save the smallest of microdisks; the radiation Q of the lowest radial order WGM of the $D \sim 4.5$ μm microdisks studied here is greater than 10^{14} at the QD emission wavelength of 1200 nm, and is greater than 10^6 for $D \sim 2.0$ μm (FEMLAB calculations are shown in chapter 7). As such, any light that is collected through free-space methods is the result of scattering of the WGM off imperfections in the microdisk [155], a relatively inefficient and non-directional process. Bulk material absorption and absorption due to surface states may also play a role, particularly when considering devices in which the Q due to surface scattering can be in excess of 10^5. This results in a situation where the more perfect the microdisk is made (through reduction in surface roughness), and the further the Q factor is improved, the more difficult it becomes to collect light from the resonant modes. Although there may be some potential in modifying the disk geometry [155, 154] to improve this situation (for example, by etching a shallow second-order grating in the microdisk surface), the ability to do this

while maintaining high Q factors could be of potential difficulty. The most successful method to date for increasing collection efficiency from semiconductor microdisk resonators seems to be placement of the collection optics in the plane of the disk [13, 14], resulting in more effective capture of the predominantly low-angle scattered light.

The fiber taper offers an attractive alternative because it provides a means to directly couple light out of the WGMs, without relying upon the weak intrinsic radiation of the microdisk or the non-directionality of surface roughness scattering. This evanescent near field coupling, which is a function of the integrated modal overlap of the microdisk and taper modes over the interaction region [50, 137], has been demonstrated to be appreciable in previous works with small diameter semiconductor microdisks [64, 69] where phase matching between the glass fiber taper waveguide and the semiconductor microdisk is not as limiting. While the fiber taper does load the cavity mode, and thus degrade its Q, the key point is that the added loss is primarily *good loss* in the sense that it can be efficiently collected into the taper mode of interest [55, 57]. This allows for the loaded Q to be maintained at a high value while simultaneously obtaining high collection efficiency [64, 69]. The situation is analogous to the case of a Fabry-Perot cavity where one mirror is intentionally made to have a slightly lower reflectivity for output coupling, which limits the Q of the cavity, but not beyond some acceptable level. While in that case, the cavity Q is fixed by the mirror reflectivities, here we have some flexibility over the Q and the amount of loading by adjusting the cavity-taper separation.

To compare free-space and fiber-taper-based collection, we use the experimental setup depicted in fig. 6.1, which consists of a fiber taper probing station that has been incorporated into a standard photoluminescence (PL) measurement setup. Passive measurements of the resonator modes are performed by connecting the input of the fiber taper to a 1200 nm band scanning tunable laser, with the polarization of the laser output at the taper-microdisk interaction region controlled using a paddle wheel polarization controller. The entire taper probing setup (motorized stages, microcavity chip, and fiber taper waveguide) is mounted onto a larger manually actuated X-Y-Z stage that is positioned underneath an ultra-long working distance objective lens (NA = 0.4). This microscope objective is part of a PL setup that provides normal incidence pumping and free-space collection from the samples. The pump laser in the majority of the measurements is a 830 nm laser diode that is operated in quasi-continuous-wave operation (280 ns pulse width, 300 ns period). The pump beam is shaped into a Gaussian-like profile by sending the laser beam through a section of single mode optical fiber, and is then focused onto the sample with a spot size that is slightly larger than the size

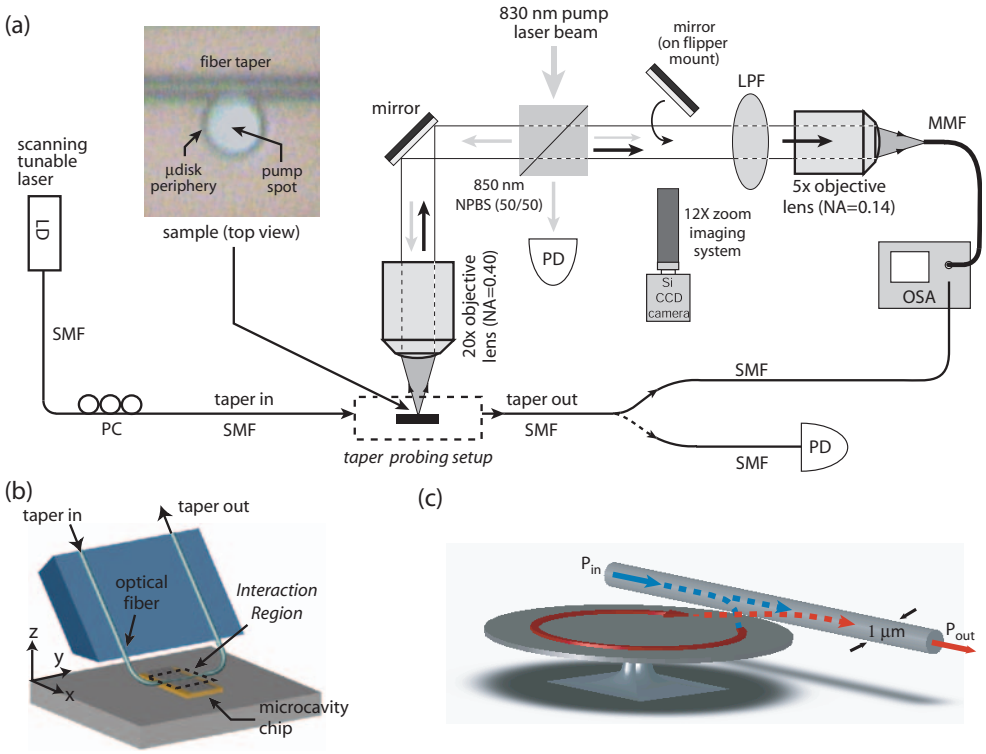

Figure 6.1: (a) Experimental setup for studying the QD-microdisk devices, where the pump laser and photoluminescence beams are shown as light gray and black arrows, respectively. The inset shows a fiber taper aligned to a microdisk that is being optically pumped from the top. Acronyms used in the diagram: polarization controller (PC), numerical aperture (NA), non-polarizing beam-splitter (NPBS), photodetector (PD), long-pass pump rejection filter (LPF), single mode fiber (SMF), multi-mode fiber (MMF), optical spectrum analyzer (OSA). (b) Schematic of the fiber taper probing geometry. (c) Schematic of the taper-to-microdisk interaction region, showing the resonant fiber taper coupling to WGMs of the microdisk.

of the microdisk (area $\sim 18\ \mu m^2$). The free-space pump laser power is monitored by using a 830 nm wavelength 50/50 non-polarizing beamsplitter (NPBS) with a calibrated photodetector (PD) on one of the ports. The QD free-space photoluminescence in the 1200 nm band is collected at normal incidence from the sample surface using the same objective lens for pump focusing, is transmitted through the 830 nm NPBS and a long-pass pump rejection filter (LPF), and is finally collected into a multi-mode fiber (MMF) using an objective lens with NA = 0.14. The luminescence collected by this MMF is wavelength resolved by a Hewlett Packard 70452B optical spectrum analyzer. For fiber taper measurements, the fiber taper is strung across the sample and positioned in the near field of the microdisk from above, allowing simultaneous (normal incidence) free-space and fiber taper optical pumping and photoluminescence collection. The output of the fiber taper can either be connected to

an InGaAs photodetector (PD) for wavelength scans using the tunable laser source, or to the OSA for analysis of the photoluminescence from the microdisk. Alignment of the pump beam and the fiber taper to the microdisk is performed by imaging through the pump and collection objective lens, as shown in the inset (a mirror flips in-and-out of the free-space photoluminescence beam path to direct the image to a 12X zoom imaging system). All of the measurements presented here were performed with the sample maintained in a room temperature environment, with no active cooling or temperature control.

This integrated setup allows for a number of different measurements to be made. Passive measurements of the microdisk resonant modes are performed by sending a tunable laser into the taper's input and monitoring the wavelength-dependent transmission at the taper's output. Photoluminescence measurements can be done in any of four potential configurations (i) free space pumping, free space collection: here, the fiber taper plays no role, and the vertically emitted power from the disks is collected into a multimode optical fiber that is then fed into the optical spectrum analyzer (OSA); (ii) free space pumping, fiber taper collection: here, the output of the fiber taper is connected to the OSA; (iii) fiber taper pumping, free space collection: here, the input of the fiber taper is connected to a fiber-coupled pump laser; (iv) fiber taper pumping, fiber taper collection: here, the free-space optics used in the standard PL measurements play no role.

6.2 Measurement of cavity Q in the 1200 nm wavelength band

The devices studied in this work have been previously characterized in the 1400 nm band, and Qs as high as 3.6×10^5 have been measured (chapter 5). Those measurements were done at wavelengths significantly red detuned from the QD emission band, where QD absorption and material absorption in the GaAs/AlGaAs waveguide layers are expected to be quite small. To confirm that the cavity Qs are still high near the ground state QD emission wavelength (peaked near 1190 nm as shown in fig. 6.2(a)), we perform passive fiber-taper-based measurements [52, 64, 69] in the 1200 nm band.[1] The high-Q resonances within the transmission spectrum (fig. 6.2(b)), under closer inspection, are seen to be doublets (inset to fig. 6.2(b)), as was the case for the measurements in the 1400 nm band shown in chapter 7.

FEMLAB solutions of the WGM resonances of the microdisks studied in this chapter show

[1]The WGMs in the 1400 nm wavelength band are expected to have very similar radiation and scattering losses as those in the 1200 nm band for the microdisk geometries studied here. Differences in Q at these two wavelengths are thus expected to be indicative of wavelength-dependent material absorption losses.

that the free spectral range (FSR) is ~ 40 nm for TE-polarized modes of low radial mode number ($q = 1,2,3,4$) in the 1200 nm wavelength band. Higher radial order WGMs ($q \geq 5$) are expected to show up only very weakly in the fiber taper transmission owing to their relatively small radiation limited Q factors ($\lesssim 10^4$) and significantly larger overlap with the support pedestal. From the broad spectral wavelength scan shown in fig. 6.2(b), a pair of deeply coupled resonant modes separated by a full FSR are observed ($\lambda \sim 1222$ and 1263 nm), as well as several other deeply coupled resonant modes. Due to the extended nature of the higher order radial modes and their better phase matching to a low-index glass waveguide such as the fiber taper, the coupling to the lowest order $q = 1$ WGM is typically lower than that of the $q = 2$ mode for similar sized microdisks [137]. We believe that these doublet modes at $\lambda \sim 1222$ nm and $\lambda \sim 1263$ nm are first order ($q = 1$) radial modes, while the mode at $\lambda \sim 1242$ nm is probably a $q = 2$ radial mode. The broader and more weakly coupled intermediate modes are most likely higher order radial modes, $q = 3,4$ (higher order slab modes in the vertical direction of microdisk are also a possibility, though less likely due to their reduced radiation Q). Examining the linewidth of the doublet resonances when the taper is relatively far away from the microdisk gives an estimate for the cold-cavity, unloaded Q of the modes. Qs as high as 2.2×10^5 at $\sim$1260 nm and as high as 1.9×10^5 at $\sim$1220 nm are measured in these microdisks (insets of fig. 6.2(b)), the latter of which is only 30 nm red detuned from the peak of the QD emission spectrum (fig. 6.2(a)). These Q factors are quite high for a wavelength-scale AlGaAs microcavity [13, 14, 71, 84, 158], and correspond to a cavity decay rate of $\kappa/2\pi \sim 0.6$ GHz for resonant modes with an effective mode volume of only $V_{\text{eff}} \sim 7(\lambda/n)^3$. Nevertheless, some degradation in the quality factors from those previously measured in the 1400 nm band is observed. These are believed to be at least in part due to absorption in the QD layers, as evidenced by the emission in the PL spectrum at these wavelengths (fig. 6.2(a)).

Additional measurements in the 980 and 850 nm wavelength bands on similar microdisk resonators formed in AlGaAs (without a QD layer) have indicated a trend of optical loss which significantly increases below a wavelength of 1 μm. This trend in optical loss is similar to that reported in ref. [66], where material absorption that extended 350 meV within the bandgap was attributed to incorporation of oxygen impurities into the AlGaAs lattice. We are currently investigating this more carefully, in a project headed by Chris Michael in collaboration with the group of Evelyn Hu at UC Santa Barbara. This wavelength-dependent loss was one of the main reasons we wanted to test the devices in the 1200 nm band as well as the 1400 nm band; fortunately, as we have seen above, the achievable Qs at 1200 nm are still quite high.

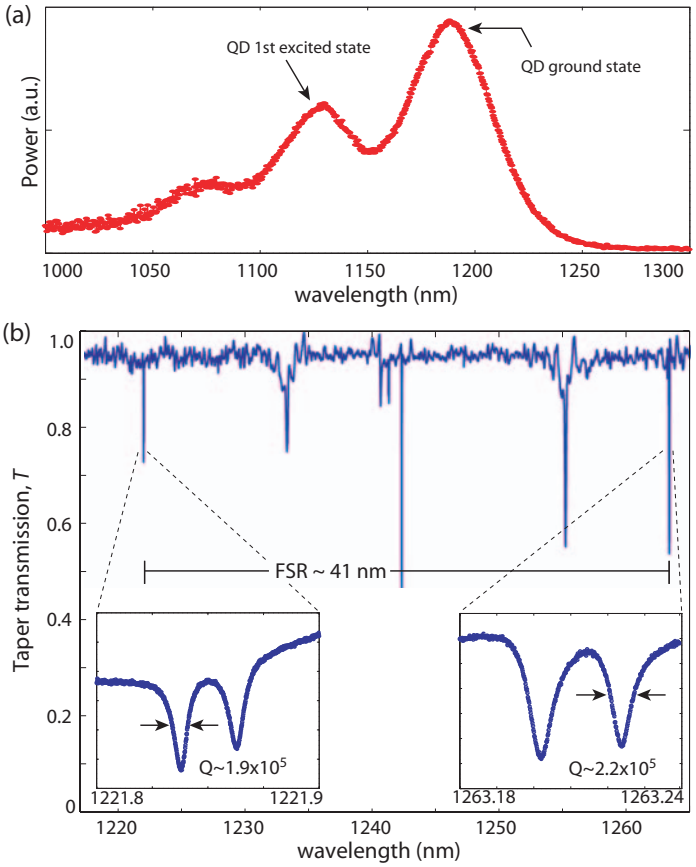

Figure 6.2: (a) Photoluminescence from an unprocessed region of the 1DWELL material. (b) Passive taper-based measurements of a microdisk in the 1200 nm band. The insets show high resolution scans for two sets of doublet modes for this device. These high resolution scans are taken when the taper-microdisk separation is a few hundred nm and the depth of coupling is $\sim 5\% - 10\%$.

6.3 Improved collection efficiency with fiber tapers

We now turn to the heart of the current work, which is a study of the gains in efficiency that can be achieved by using optical fiber tapers as a collection tool in PL measurements. This is initially done by comparing the amount of power obtained in free-space and fiber taper collection configurations, while maintaining identical free-space pumping conditions (in terms of pump-beam intensity and pump beam position). The free-space collection for a microdisk that has been pumped at normal incidence with ~ 580 W/cm^2 at 830 nm is shown in fig. 6.3(a). This pump intensity is near the laser threshold for this device (see below), and we see that the peak height at $\lambda \sim 1193.5$ nm is ~ 30 pW. For comparison to the fiber taper collection described below, an estimate of the optical losses in the free-space collection setup were made (after removal of the pump rejection filter). By measuring the collected pump laser power reflected off of the mirror-quality surface of the AlGaAs epitaxy, and assuming a 30% reflection coefficient from the AlGaAs surface, 43% of the reflected pump beam was collected into the OSA. Additional limitations in the normal incidence free-space collection stem from the finite numerical aperture of the collecting lens (NA=0.4) which covers only 4% of

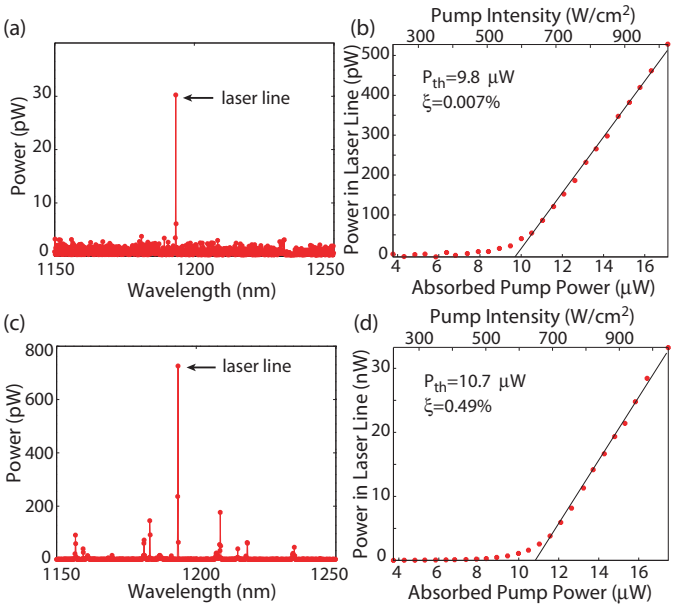

Figure 6.3: (a) Emission spectrum and (b) Light-in-light-out (L-L) curve for normal incidence free-space collection from a (free-space) optically pumped microdisk. Fiber taper collected (c) emission spectrum and (d) L-L curve from the same microdisk resonator, under identical pumping conditions. The emission spectra were taken near laser threshold at $\sim$ 580 W/cm^2 of incident pump beam intensity. The fiber taper collected power includes that from the forward propagating transmission channel only.

the full 4π steradians.

Next, we consider the use of the optical fiber taper as a collection optic in the PL measurements. To obtain an estimate of the amount of coupling between the taper and the microdisk, the free-space pump beam is blocked, and passive measurements at wavelengths that are slightly red detuned from the QD emission are performed as described above in section 6.2. Since the FSR for the low radial number WGMs of the microdisks studied here is $\sim$ 41 nm in the 1200 nm wavelength band, the modes coupled to and studied passively are typically a single FSR red detuned from the lasing mode. For most experiments, the taper is placed in direct contact with the top edge or side of the microdisk, which increases the amount of coupling from that shown in fig. 6.2(b) to transmission depths between 30% and 60%. For this initial measurement, a resonance depth of $\sim$38% is obtained for a cavity mode at $\lambda \sim 1238.1$nm, which gives us a qualitative estimate for the coupling to WGMs overlapping the peak of the gain spectrum.[2] This coupling depth corresponds to a taper collection efficiency $\eta_0 \sim 11\%$, where η_0 is defined (ref. [57] and appendix E) as the fraction of the optical power from the cavity resonant mode that is coupled into the fundamental fiber taper mode in the forward propagating transmission direction. Other loss channels from the microdisk include intrinsic loss of the cavity in absence of the taper, parasitic coupling into higher-order, non-collected modes of the fiber taper, and for the standing wave modes studied here, coupling into the backwards

[2]The coupling between the taper and microdisk can be different for different cavity modes, so this technique is used primarily as a qualitative guide.

propagating fundamental taper mode. For the moderate coupling depths measured here, the taper coupling efficiency into the forward and backward propagation directions is approximately equal, thus yielding an overall taper coupling efficiency of $\eta_0' \sim 22\%$ for this WGM.

Once this level of coupling has been achieved, the tunable laser output is blocked, the free-space pump beam is unblocked, and the output of the fiber taper is disconnected from the photodetector and connected to the OSA to measure the emitted power from the microdisk. fig. 6.3(c) shows the resulting spectrum collected by the fiber taper in the forward propagating transmission direction. We see that at the wavelength $\lambda \sim 1193.5$ nm, the peak height is ~ 725 pW, which is nearly a factor of 25 times improvement over the peak height observed in normal incidence free-space collection. In addition, a significant amount of power is present within modes that were not detectable in the free-space case (the noise floor of the OSA was approximately 1 pW), due to the poor efficiency of collection in this configuration.

This straightforward comparison of the collected powers for a single pump power is not necessarily the most appropriate comparison, however. The reason for this is that the fiber taper loads the cavity, thus decreasing the Q of the resonant modes and increasing the threshold pump power, so that for a given pump power the laser is not equally above threshold in the two measurements. Another, more appropriate comparison is the differential collection efficiency above threshold, which we label ξ. This is determined by measuring a light-in-light-out (L-L) curve for the microdisk and taking the slope of this curve above threshold. In these curves, the light out is taken to be the total power within the laser line, while the light in is taken to be the estimated absorbed pump power. The absorbed pump power is determined by multiplying the pump beam intensity by the area of the microdisk to get an incident pump power (the beam overlaps the entirety of the disk), and then multiplying this value by the absorption of the microdisk at 830 nm. We estimate this absorption to be $\sim 10\%$, assuming an absorption coefficient of 10^4 cm^{-1} in the GaAs, quantum well, and QD layers [152], and a reflection coefficient of 30% at the GaAs-air interfaces at the top and bottom of the disk. The resulting L-L curves are shown in fig. 6.3(b),(d) for both free-space and fiber-taper collection. We see that the threshold pump power has indeed increased in the case of fiber-taper collection, but that the differential efficiency has also significantly improved and is more than 70 times that of the free-space value.

To study the tradeoffs between ξ and threshold more closely, in fig. 6.4(a) several L-L curves are plotted, each for a different taper position with respect to the microdisk (note that the microdisk studied here is not the same as the one studied above, but the qualitative behavior is identical). The

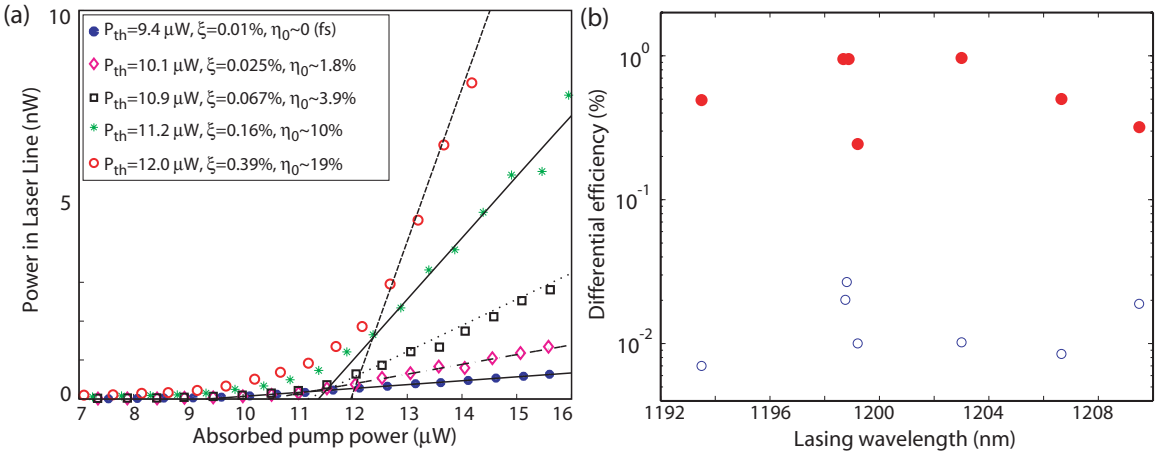

Figure 6.4: (a) L-L curves for free-space pumping and fiber taper collection at different taper positions. For each curve, we note the threshold pump power (P_{th}), the fiber taper collection efficiency (η_0) for a mode that is red detuned from the peak QD emission, and the above threshold differential efficiency (ξ). (b) Scatter plot of the differential efficiency for fiber taper (filled circles) and free-space collection (open circles) for a number of different microdisk lasers. For these measurements the fiber taper collected power included that from the forward propagating transmission channel only.

different taper positions correspond to a varying level of coupling between the microdisk and taper, which we again qualitatively estimate through measurements of the coupling to a microdisk WGM that is red detuned from the QD emission in the 1200 nm band. From fig. 6.4(a), we see that in general, both the threshold power and ξ increase with increasing η_0. As might be expected, in the course of these measurements it was possible in some cases to load the microdisk strongly enough to degrade the initial laser mode's *Q* to the point that it no longer lases, and a different mode (with a higher loaded *Q*) begins to lase.

A number of different microdisk devices have been studied, and the results described above are fairly consistent from device to device, with ξ routinely 1-2 orders of magnitude larger when fiber taper collection is employed. A scatter plot for some of this data is shown in fig. 6.4(b). Despite the significant improvement obtained using the fiber taper, we see that the largest ξ measured is roughly 10 nW/μW, which means that only 1% of the pump photons are converted to a collected signal photon, and we should thus consider why ξ is far below unity. We first note that when considering collection into both directions of the fiber taper, ξ is actually 2% for the standing wave WGMs of the microdisks studied here. A measure of the fiber taper collection efficiency of the microdisk WGM laser light, η_0, from the passive wavelength scans described above indicate that the external

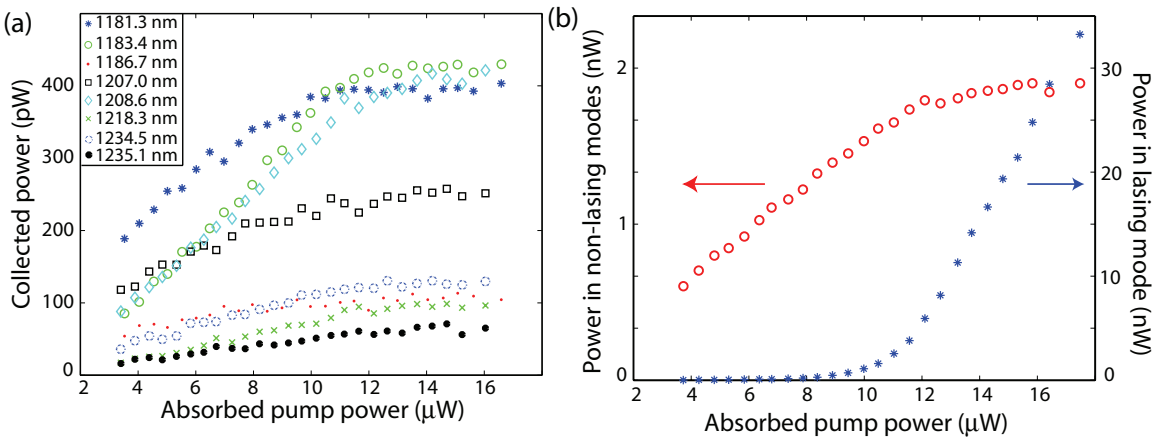

Figure 6.5: (a) L-L curves for non-lasing modes of the disk studied in fig. 6.3. (b) Total power in the non-lasing modes (shown by open circles), showing saturation for pump values close to the threshold value for the lasing mode (shown by asterisks). Note that the y-axis scale for the lasing mode is 15 times larger than that for the non-lasing modes.

fiber taper collection efficiency should be as high as $\sim 22\%$ (corresponding to 11% for the forward transmission direction only). The total loss through the fiber taper and all of the fusion-splices and connections in the fiber path was measured to be ~ 1.6dB, so that, if symmetric loss in the taper about the microdisk coupling region is assumed, $\sim 17\%$ of the WGM laser photons collected by the taper are lost before they reach the OSA. Taken together, these two factors put an estimate of the upper bound on the fiber-coupled external laser efficiency of 18% for collection into both directions of the fiber.

The roughly order of magnitude difference between the measured (2%) and expected (18%) differential laser efficiency may be a result of several factors involving the complex dynamics within the DWELL active region. Previous measurements of DWELL injection lasers in stripe geometries [144] indicate that the internal quantum efficiency of the quantum dots is $\eta_i^{QD} \sim 0.5$ (this is roughly the percentage of carriers captured by the QDs in the DWELL structure that contribute to stimulated emission above threshold). This factor can certainly change from growth to growth, and given that the laser threshold values are roughly 2-2.5 times higher than that measured in previous work on identically fabricated devices from a different wafer growth [69], we might qualitatively expect ξ to be reduced by a factor of $\sim 4-5$ due to η_i^{QD}.

Both the spectral and spatial distribution of carriers within the microdisk may also lead to reductions in the laser differential efficiency through incomplete clamping of the spontaneous emission into the non-lasing modes of the microdisk above threshold. To examine such effects in our struc-

tures, we measure L-L curves (fig. 6.5(a)) for a number of the most prominent non-lasing WGMs of the microdisk studied in fig. 6.3. We see that the emission into these modes is largely clamped above the threshold for the lasing mode (estimated to be 10.7μW of absorbed pump power). The aggregate effect is clearly seen in fig. 6.5(b), where the power into the non-lasing WGMs has been summed and plotted along with the L-L curve for the lasing mode. Such clamping has been reported by other authors for similarly sized microdisks [159], while smaller microcavity devices with a larger laser mode spontaneous emission rate, have exhibited a gradual rollover and/or incomplete clamping of spontaneous emission [120, 159, 160, 43]. Measurement of the background spontaneous emission into non-WGM, radiation modes of the microdisk was performed using free-space collection (the fiber taper is much more sensitive to WGM emission than to emission from the center of the microdisk into radiation modes), and did show incomplete clamping of the spontaneous emission. This sort of spatial hole burning has been predicted in numerical modeling of microdisk cavities [161]. If this is the case, the effective pump area is limited to a region about the WGM. Assuming that the WGM radial width is approximately (λ/n_{eff}), where n_{eff} is the effective refractive index in the plane of the microdisk,[3] this corresponds to a $7\mu\text{m}^2$ area in the devices under test here. Since the total disk area is $\sim 16\mu\text{m}^2$, then only $7/16$ of the pump photons would be effectively pumping the WGM. Including this factor brings the expected value of ξ within the range of experimentally measured values.

Aside from reducing taper loss (loss < 0.5dB can be easily achieved in our lab), η_0 is the main parameter that can be improved upon to increase ξ. This can be done by adjusting the geometry of the disk (using thinner disks, for example) to bring the index of the WGMs of the semiconductor microdisks closer to that of the silica fiber taper, so that more efficient coupling can be obtained. A study of such modifications in Si microdisk structures has been undertaken, and the regimes of critical coupling and overcoupling have been achieved [137]. In addition, if spatial hole burning is significant, another factor that could potentially be improved is the method of pumping. In particular, the pumping beam could be shaped to preferentially pump the perimeter of the microdisk (i.e., an annular-shaped beam could be used). Alternately, as discussed below, a fiber taper could be used to pump the microdisk.

[3] Finite-element simulations have shown this to be an accurate estimate.

6.4 Fiber-pumped microdisk lasers

In addition to improving the collection efficiency, optical fiber tapers have the potential for improving the pump efficiency of these QD-containing microdisks; such an effect has in fact been demonstrated in previous work on doped glass microcavities [162, 73, 74]. In particular, if the pump laser is resonant with a WGM of the microdisk, light can be absorbed with high efficiency, and in the case of critical coupling, complete power transfer can be achieved. This should be contrasted with the case of free-space pumping, where only a small percent (10% for the devices we have considered here) of the incident pump light is absorbed by the device, and some of this absorption is in a region (the center of the microdisk) that does not contribute to useful gain for the resonant WGMs [161].

For an initial demonstration, we use a tunable laser operating in the 980 nm band as a pump source. The 830 nm pump laser is not used because the absorption within the microdisk at this wavelength is too large to allow uniform pumping of the microdisk perimeter, as the pump light is absorbed before a single round trip around the cavity can be made. At 980 nm, the material absorption is still relatively high (the quantum well layer will be highly absorbing), so that the Q_{980} of WGM modes near the pump wavelength are not expected to exceed a few hundred. The pump laser is connected to the fiber taper input, and the fiber taper output is connected to the OSA. The taper is contacted to the side of the microdisk, and the pump wavelength and polarization are manually adjusted until the collected power in the OSA is maximized (this is necessary in order to resonantly couple to a mode within the pump wavelength band). A typical L-L curve and subthreshold spectrum are shown in fig. 6.6. We see that a significant amount of power is collected into the fiber taper, and that in particular, the subthreshold spectrum shows a number of well-resolved modes with a good signal-to-noise ratio. The estimated absorbed pump power in the microdisk displayed in fig. 6.6(a) corresponds to 66% of the input power in the fiber taper, and is found by taking the difference in the 980 nm band taper transmission between when the taper is displaced tens of microns above the microdisk (no coupling) and when it is in contact with the microdisk (strongly coupled). We note that the pump threshold value in this pumping geometry is only about a factor of two less than the *incident* pump power in the 830 nm free-space pumping, and is significantly larger than what might be expected (ideally, the pump power here should be less than the *absorbed* pump power in the 830 nm pumping). This is most likely a result of the relatively crude method we have employed to estimate the power absorbed in the microdisk; a much more accurate method for determining the coupled pump power uses the wavelength-dependent transmission of the

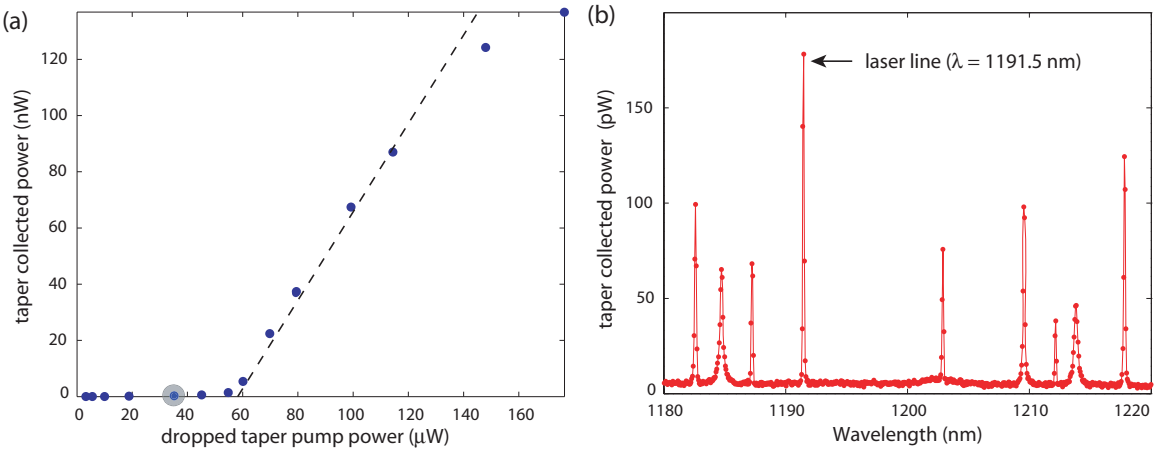

Figure 6.6: (a) L-L curve for a QD-microdisk device where the fiber taper is used for both pumping (at $\lambda = 967.6$ nm) and collection. The absorbed power was estimated to be 66% of the input power in the fiber taper. (b) Sub-threshold spectrum for this device taken at an estimated absorbed power of 37 μW (highlighted point in (a)).

fiber taper to map out the resonance line due to the WGM at the pump wavelength. Here, the strong absorption of the microdisk in the 980 nm band makes it difficult to separate resonantly coupled power from scattering losses at the taper-microdisk junction. In order to more carefully study the efficiency of this fiber-pumping and fiber-collecting configuration, experiments in which an excited state of the quantum dots is resonantly pumped through the fiber taper are currently underway.

6.5 Discussion and future applications

As mentioned in the introduction, efficient optical access to wavelength-scale microcavities is of great importance to quantum optics and information processing applications currently being investigated within cavity QED systems. In almost any application involving the coherent transfer or manipulation of quantum information, loss is a significant detriment. As described in ref. [68], current implementations of linear optics quantum computing require a near-unity collection efficiency of emitted photons from a single photon source. The same is true for applications involving quantum repeaters in a quantum network [141]. A solution that is often proposed is to embed the single photon emitter within a microcavity with a high spontaneous emission coupling factor β, so that the majority of emitted photons are coupled into the microcavity mode. However, it is important to note that even for a $\beta = 1$ microcavity, it is still necessary to have a method to effectively collect all of the photons that are radiated by that one cavity mode [163]. Also, from a very practical perspec-

tive, efficient collection of emitted light from a microcavity is of premium importance for optical telecommunication wavelengths $> 1\mu m$, where the dark count rates from single photon counters are often 2-3 orders of magnitude larger than the Si single photon counters used at shorter wavelengths [164].

An efficient coupling channel can also enable a number of different types of experiments. Having access to this coupling channel makes the cavity transmission (and reflection) an experimentally accessible parameter whose behavior can be monitored to detect signatures of specific types of system behavior. In recent experimental measurements of coupling between a single quantum dot and a resonant mode of a semiconductor microcavity [71, 158, 70, 16, 109], spontaneous emission from the coupled system is the only parameter measured. Alternatively, using fiber tapers, vacuum Rabi splitting can be detected by simply measuring the transmission through the cavity as a function of the input wavelength to the cavity; such an experiment is directly analogous to the experiments done with cooled alkali atoms coupled to a Fabry-Perot cavity [77, 78]. Non-linear effects, such as optical bistability and photon blockade, and coherent control of the quantum system are also more easily observed through the optical transmission or reflection channel of a microcavity. Perhaps most importantly, by knowing the precise level of coupling between the fiber taper and the microcavity, the number of photons injected into the cavity can be precisely calibrated. This is obviously of paramount importance in experiments that involve few or single cavity photons. Finally, we note that although many of the advantages we have described are also applicable to in-plane waveguides that are microfabricated next to the cavities, the fiber taper provides a level of flexibility that, for example, allows for rapid device characterization, as described in detail in ref. [54].